

THE AGES OF THE THIN DISK, THICK DISK, AND THE HALO FROM NEARBY WHITE DWARFS

MUKREMIN KILIC¹, JEFFREY A. MUNN², HUGH C. HARRIS², TED VON HIPPEL^{3,4}, JAMES W. LIEBERT⁵, KURTIS A. WILLIAMS⁶, ELIZABETH JEFFERY⁷, STEVEN DEGENNARO⁸

Draft version September 16, 2018

ABSTRACT

We present a detailed analysis of the white dwarf luminosity functions derived from the local 40 pc sample and the deep proper motion catalog of Munn et al. (2014, 2017). Many of the previous studies ignored the contribution of thick disk white dwarfs to the Galactic disk luminosity function, which results in an erroneous age measurement. We demonstrate that the ratio of thick/thin disk white dwarfs is roughly 20% in the local sample. Simultaneously fitting for both disk components, we derive ages of 6.8-7.0 Gyr for the thin disk and 8.7 ± 0.1 Gyr for the thick disk from the local 40 pc sample. Similarly, we derive ages of 7.4-8.2 Gyr for the thin disk and 9.5-9.9 Gyr for the thick disk from the deep proper motion catalog, which shows no evidence of a deviation from a constant star formation rate in the past 2.5 Gyr. We constrain the time difference between the onset of star formation in the thin disk and the thick disk to be $1.6^{+0.3}_{-0.4}$ Gyr. The faint end of the luminosity function for the halo white dwarfs is less constrained, resulting in an age estimate of $12.5^{+1.4}_{-3.4}$ Gyr for the Galactic inner halo. This is the first time ages for all three major components of the Galaxy are obtained from a sample of field white dwarfs that is large enough to contain significant numbers of disk and halo objects. The resultant ages agree reasonably well with the age estimates for the oldest open and globular clusters.

Subject headings: white dwarfs – stars: luminosity functions

1. INTRODUCTION

There are a variety of methods for measuring the ages of stars and the populations that they reside in. Traditionally the best age measurements have come from fits to the main-sequence turn-offs in open and globular clusters, which reveal ages of up to ~ 12 Gyr for the oldest globular clusters. The same technique can be applied to field stars if accurate trigonometric parallaxes are available. For example, using Hipparcos parallaxes of turn-off field stars and subgiants, Liu & Chaboyer (2000) and Sandage et al. (2003) derive metallicity-dependent solar neighborhood disk ages of $7.5 - 7.9 \pm 0.7$ Gyr.

Gyrochronology can be used to age-date clusters as old as 4 Gyr with a precision of ~ 0.7 Gyr (Barnes et al. 2016). However, Angus et al. (2015) find unexpected deviations from the predicted age versus rotation period relation and they demonstrate that the age uncertainties are significantly higher for field stars.

Nucleocosmochronometry, the use of thorium and uranium to infer ages of metal-poor halo stars, provide ages with an uncertainty of 2-3 Gyr for 13 Gyr old halo stars

(Snedden et al. 2003; Frebel et al. 2007). There is no single method that works well for a broad range of stellar types or ages (Soderblom 2010), and each method has its own theoretical (e.g., incomplete treatments of convection and rotation for main-sequence stars) and observational (e.g., small sample size, uncertainties in abundances, distances, and reddening) problems that limit the age precision.

White dwarfs offer an independent technique for measuring stellar population ages. The surface temperature and luminosity of a white dwarf is primarily a function of its age, and secondarily a function of its mass, interior and surface composition. Schwarzschild (1958) estimated a luminosity of $10^{-4}L_{\odot}$ for an 8 Gyr old white dwarf. Winget et al. (1987) and Liebert et al. (1988) demonstrate that the lack of stars fainter than this luminosity in the Solar neighborhood is due to the finite age of the Galactic disk, which Leggett et al. (1998) constrain to be 8 ± 1.5 Gyr based on 43 stars. Hansen et al. (2004, 2007, 2013) extended white dwarf cosmochronology to the halo by using *Hubble Space Telescope* observations of the globular clusters M4, NGC 6397, and 47 Tuc, and derived ages of ≥ 10.3 , 11.5 ± 0.5 , and 9.9 ± 0.7 Gyr, respectively. Similarly, Kilic et al. (2012) and Kalirai (2012) constrain the ages of six kinematically-confirmed field halo white dwarfs to 11-11.5 Gyr.

Recent large scale proper motion surveys (Munn et al. 2004; Harris et al. 2006; Rowell & Hambly 2011; Limoges et al. 2015) provide an excellent opportunity to create accurate luminosity functions for the disk. In addition, the proper motion survey of Munn et al. (2014, 2017) goes deep enough ($r = 21.5$ mag) to uncover a sizable fraction of halo white dwarfs. Here we take advantage of this latter survey to constrain, for the first time, the ages of the thin disk, thick disk, and the halo

¹ Homer L. Dodge Department of Physics and Astronomy, University of Oklahoma, 440 W. Brooks St., Norman, OK, 73019

² US Naval Observatory, Flagstaff Station, 10391 W. Naval Observatory Road, Flagstaff, AZ 86005

³ Center for Space and Atmospheric Research, Embry-Riddle Aeronautical University, Daytona Beach, FL 32114

⁴ Max Planck Institute for Astronomy, Königstuhl 17, 69117 Heidelberg, Germany

⁵ University of Arizona, Steward Observatory, Tucson, AZ 85721

⁶ Department of Physics and Astronomy, Texas A&M University-Commerce, P.O. Box 3011, Commerce, TX 75429

⁷ Department of Physics and Astronomy, Brigham Young University, N283 ESC, Provo, UT 84602

⁸ Department of Astronomy, University of Texas at Austin, 1 University Station C1400, Austin, TX 78712

from the same sample of white dwarfs. In Section 2 we describe the input model white dwarf luminosity functions, and in Section 3 we present an analysis of the local 40 pc white dwarf sample (Limoges et al. 2015). In Section 4, we analyze the disk and halo luminosity functions from the deep proper motion survey of Munn et al. (2014, 2017) and present new age constraints for the three major components of the Galaxy. We compare these white dwarf age constraints with previous age measurements from the literature and highlight the next generation of surveys that will improve these age constraints in Section 5.

2. MODEL LUMINOSITY FUNCTIONS

2.1. Thin Disk

The canonical age estimates for the thin disk, thick disk, and halo range from about 7 Gyr for the disk to about 13 Gyr for the halo. Cignoni et al. (2006) and Tremblay et al. (2014) find an approximately constant or a modestly rising star formation rate history in the Galactic disk. For simplicity, we assume a constant star formation rate for the thin disk. We generate 100 main-sequence stars at every 1 Myr timestep with masses randomly drawn between 0.8 and $8 M_{\odot}$ from a Salpeter mass function with exponent $\alpha = 2.35$ (Salpeter 1955). This mass range encompasses the progenitors of all white dwarfs that would have formed in the past 13 Gyr of Galactic history. We run the simulations until the required age for each luminosity function is reached, thereby creating 1.3 million stars for the 13.0 Gyr model.

We assume solar metallicity for the thin disk stars and use the main-sequence lifetimes from the stellar evolution calculations by Hurley et al. (2000). For the stars that evolve into a white dwarf within the age of a given model, we use the initial-final mass relation from Kalirai et al. (2008) to estimate the final masses. The model luminosity function age minus the formation time of the main-sequence star minus the main-sequence lifetime gives the white dwarf cooling age of each star. We then use the evolutionary models by Fontaine et al. (2001) to calculate the bolometric magnitude of each white dwarf, and bin the luminosity function with the same binning as the observational sample studied. We create disk luminosity functions with ages ranging from 6 to 13 Gyr, with a resolution of 0.1 Gyr.

Figure 1 shows theoretical thin-disk luminosity functions for an age of 10.0 Gyr for pure H (solid line) and pure He (dashed line) white dwarfs. The two luminosity functions are remarkably similar for $M_{\text{bol}} < 15$ mag, which corresponds to $T_{\text{eff}} \geq 5000$ K. Both pure H and pure He atmosphere white dwarfs with $M = 0.6 M_{\odot}$ take 6.5 Gyr to reach $M_{\text{bol}} = 15$ mag. On the other hand, a pure H atmosphere white dwarf takes 0.7 and 0.8 Gyr longer than a pure He atmosphere white dwarf to cool down to $M_{\text{bol}} = 16$ and 16.5 mag, respectively. Hence, the choice of H/He atmospheres affects the faint end of the luminosity function for $M_{\text{bol}} > 15$ mag and $T_{\text{eff}} \leq 5000$ K.

The overall fractions of DA and DB white dwarfs in the solar neighborhood are 80% and 20%, respectively (e.g. Limoges et al. 2015). However, the evolution of the surface composition of white dwarfs is not well understood (Bergeron et al. 2001). This is especially a prob-

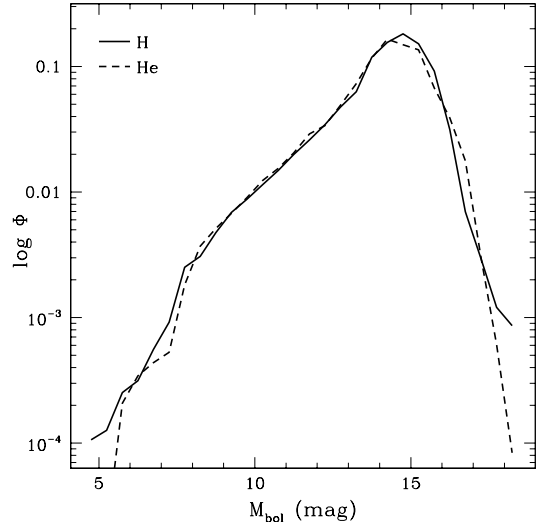


FIG. 1.— Model luminosity functions for 10.0 Gyr old thin disk populations of pure H (solid line) and pure He atmosphere (dashed line) white dwarfs.

lem when both He and H become invisible below 5,000 K. Using the state-of-the-art white dwarf model atmospheres that include the Lyman α red wing opacity, Kowalski & Saumon (2006) demonstrate that most or perhaps all of the cool DC white dwarfs have hydrogen-rich atmospheres (see the discussion in Limoges et al. 2015). Since these stars define the faint end of the luminosity function, and therefore the age of a given population, we use the evolutionary models for pure H atmosphere white dwarfs throughout our simulations. We discuss the choice of H versus He atmospheres further in section 4.3, where we demonstrate that the addition of He atmosphere stars ($\sim 20\%$ He fraction) has a negligible effect on our age measurements.

2.2. Thick Disk and Halo

There are significant differences between the star formation history and metallicity of the thin disk, thick disk, and the halo. Ivezić et al. (2008) used Sloan Digital Sky Survey photometry for more than 2 million F/G stars to derive $[\text{Fe}/\text{H}] = -0.7$ and -1.5 for the thick disk and halo, respectively. The thick disk is a relatively old population (~ 10 Gyr) with the bulk of the stars forming over a relatively short period of time of ~ 1 Gyr. Similarly, the Galactic halo is also best described by a single star burst model lasting over 1 Gyr with an age of ~ 12 Gyr (Reid 2005).

To assemble the model luminosity functions for the thick disk and halo, we use a top-hat star formation rate; we generate 1000 main-sequence stars at every 1 Myr timestep with masses randomly drawn between 0.75 and $8 M_{\odot}$ from a Salpeter mass function, and run the simulations for 1 Gyr after the formation of each population, creating 1 million stars in the process. We use the evolutionary models by Hurley et al. (2000) for the thick disk and halo metallicities to estimate the main-sequence lifetimes. We then follow the same procedure as described in the previous section to estimate the final white dwarf mass, cooling age, and the bolometric magnitude. We create thick disk (halo) luminosity functions with ages

ranging from 8 to 13 (15) Gyr, with a resolution of 0.1 Gyr.

There are marked differences between the model luminosity functions for the populations with different metallicities and star formation histories. Hurley et al. (2000) predict main-sequence lifetimes of 1164, 909, and 767 Myr for $2M_{\odot}$ thin disk, thick disk, and halo stars, respectively. For an 8 Gyr old population with the star formation histories discussed above, 44.3% of the thin disk stars with masses $0.8 - 8M_{\odot}$ have already turned into white dwarfs, whereas this number is significantly higher for the thick disk and the halo; 73.0% and 79.5%, respectively. In addition, the thick disk and halo luminosity functions peak at fainter magnitudes. For an 8 Gyr old population, 76.5% of the thin disk white dwarfs and 91.6% of thick disk white dwarfs have $M_{\text{bol}} > 13$ mag, respectively.

3. THE 40 PC SAMPLE

3.1. Previous Work

Limoges et al. (2015) performed a detailed model atmosphere analysis of the local 40 pc white dwarf sample and constructed a luminosity function based on 501 objects. Comparing this luminosity function to the theoretical luminosity functions from Fontaine et al. (2001), Limoges et al. (2015) find a significant bump around $M_{\text{bol}} \sim 10$ mag and attribute this to an enhanced star formation rate about 300 Myr ago. Based on the observed cut-off in the luminosity function, they also find a Galactic disk age of around 11 Gyr. We note that the theoretical luminosity functions used in that work rely on simplified versions of the initial-final mass relation and main-sequence lifetimes, specifically $M_{\text{WD}} = 0.4e^{0.125M}M_{\odot}$ and $t_{\text{MS}} = 10M^{-2.5}$ Gyr.

Torres & García-Berro (2016) revisit the analysis of the 40 pc sample with a population synthesis code. They draw their sample of stars from a Salpeter mass function, use the initial-final mass relation of Catalán et al. (2008), and cooling tracks of Renedo et al. (2010) and Althaus et al. (2007). Using the observed cut-off of the luminosity function, they derive an age of 8.9 ± 0.2 Gyr and they also explain the bump around $M_{\text{bol}} = 10$ mag as a burst of star formation 600 Myr ago. They test the reliability of their results against the assumed initial mass function and the initial-final mass relation, and conclude that the age measurement is insensitive to these input parameters, except for extreme slopes for the initial-final mass relation. However, their best-fit model significantly overpredicts the number of white dwarfs near the maximum of the luminosity function. Torres & García-Berro (2016) can explain this discrepancy with an initial-final mass relation that has a slope 30% larger than the observed relation for stars more massive than $4M_{\odot}$ from Catalán et al. (2008). However, there is no evidence for such a steep initial-final mass relation (Kalirai et al. 2008; Williams et al. 2009), and we find this explanation unlikely. Instead, we suggest a simpler explanation for the discrepancy; the neglected contribution of thick disk white dwarfs to the faint end of the luminosity function.

3.2. Thick Disk Number Density

Studying the 3D space motions of 398 field DA white dwarfs from the Supernovae Ia Progenitor Survey,

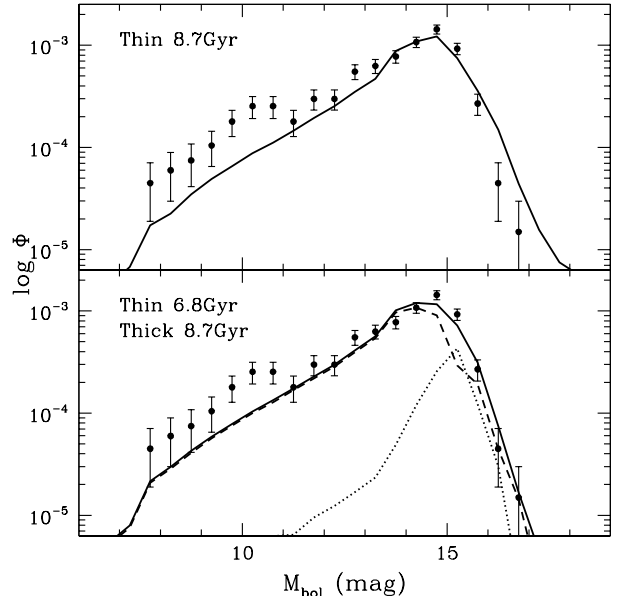


FIG. 2.— The observed luminosity function for the local 40 pc sample of white dwarfs (points with error bars, Limoges et al. 2015) compared to the best-fit synthetic white dwarf luminosity function (solid lines). The top panel shows the model fits assuming a population of 100% thin disk stars, whereas the bottom panel shows the fits using a composite population where the ratio of thick disk to thin disk white dwarfs is 22%. Dashed and dotted lines show the contribution from the thin disk and thick disk white dwarfs, respectively.

Pauli et al. (2006) find that 7% of the white dwarfs in their sample belong to the thick disk. Reid (2005) argue that the fraction of thick disk white dwarfs in the local population could be as high as $\sim 20\%$ given that it is an old population that leads to an enhanced number of low luminosity objects. Since chemical-tagging of white dwarfs as thick disk objects is not possible, identifying individual objects as thick disk members is difficult without accurate parallaxes and constraints on their 3D space motions. Rowell & Hambly (2011) rely on a statistical approach to disentangle the thin disk and thick disk luminosity functions, and find that the thick disk and halo contribute roughly 16% and 5% of the local white dwarfs, respectively. Due to small number statistics at the faint end of their luminosity functions, they do not attempt age measurements for the different populations, but they conclude that traditional approaches that do not account for a significant contribution from thick disk and halo stars cannot measure an accurate thin disk age.

Based on star counts from the SDSS, Jurić et al. (2008) measure a local density ratio of $\rho_{\text{thick}}/\rho_{\text{thin}} = 12 \pm 1\%$ for main-sequence stars. de Jong et al. (2010) find a similar ratio, $15 \pm 4\%$, from the Sloan Extension for Galactic Understanding and Exploration (SEGUE) survey. For an 8 Gyr old thin disk that has continuous star formation, 44.3% of the stars with $M = 0.8 - 8M_{\odot}$ turn into white dwarfs, whereas for a 10 Gyr old thick disk that formed stars in the first Gyr, 80.2% are now white dwarfs. Hence, the expected number density of thick versus thin disk white dwarfs would be $12\% \times \frac{80.2\%}{44.3\%} = 21.7\%$ for a kinematically unbiased sample. However, the 40 pc sam-

ple has a lower proper motion limit of 40 mas yr^{-1} , which reduces the expected number of thin disk stars by $\approx 1.8\%$ according to the Besançon Galaxy model (Robin et al. 2012). Hence, the expected ratio of thick versus thin disk white dwarfs is 22.1% in the 40 pc sample.

3.3. Thin Disk and Thick Disk Ages

Figure 2 shows the 40 pc white dwarf luminosity function from Limoges et al. (2015) kindly made available to us by P. Bergeron. To avoid the bump around $M_{\text{bol}} = 10$ mag due to the enhanced star formation rate in the past 600 Myr (Torres & García-Berro 2016), we only use the stars with $M_{\text{bol}} > 11$ mag in our fits. Since we are mainly interested in the age constraints from the faint end of the luminosity function, we do not try to model this bump, as it has no effect on our age constraints. The top panel shows our fits assuming a population of thin disk stars only. The best fit thin disk age is 8.7 ± 0.1 Gyr, which is consistent with 8.9 ± 0.2 Gyr as measured by Torres & García-Berro (2016). However, this age measurement is clearly wrong since it ignores the contribution of thick disk stars and it assumes solar metallicity for all objects in the sample.

We show the best-fitting thin disk + thick disk composite luminosity function, as well as the contributions from both populations in the bottom panel. For $\rho_{\text{thick,WD}}/\rho_{\text{thin,WD}} = 22\%$, the best-fitting model has ages of 6.8 ± 0.2 and 8.7 ± 0.1 Gyr for the thin disk and thick disk, respectively. The composite thin+thick disk model is a significantly better fit than a thin-disk only model ($\chi^2_{\text{red}} = 1.6$ versus 3.5). In addition, the age constraints are insensitive to the assumed thick/thin disk fraction as long as this fraction is above a few per cent.

We note that the uncertainties in the age estimate comes from a Monte Carlo analysis where we replace the measured space density ϕ with $\phi + g\delta\phi$, where $\delta\phi$ is the error in space density and g is a Gaussian deviate with zero mean and unit variance. For each of 1,000 sets of modified luminosity functions, we find the model that provides the lowest χ^2 fit, and we take the range in age that encompasses 68% of the probability distribution function as the 1σ uncertainties.

To test the sensitivity of our age measurements to the specific binning used by Limoges et al. (2015), we create a new luminosity function for the 40 pc sample where the bin centers are shifted by 0.25 mag. Using the stars with $M_{\text{bol}} > 11$ mag and assuming a thick/thin disk ratio of 0.22, we derive ages of $7.0^{+0.1}_{-0.2}$ Gyr and 8.6 ± 0.1 Gyr for the thin disk and thick disk, respectively. Hence, the derived ages are not sensitive to the binning used in the luminosity function, and they are constrained to be 6.8-7.0 Gyr and 8.6-8.7 Gyr for the thin disk and thick disk, respectively.

4. THE DEEP PROPER MOTION SURVEY SAMPLE

4.1. The Disk Luminosity Function

Munn et al. (2014) presented a $\sim 3,000$ square degree deep proper motion survey reaching a limiting magnitude of $r = 21 - 22$ mag. Munn et al. (2017) identify 8472 white dwarf candidates in this survey, and use 2839 stars with $M_{\text{bol}} = 5.5 - 17$ mag to create a disk white dwarf luminosity function. To avoid contamina-

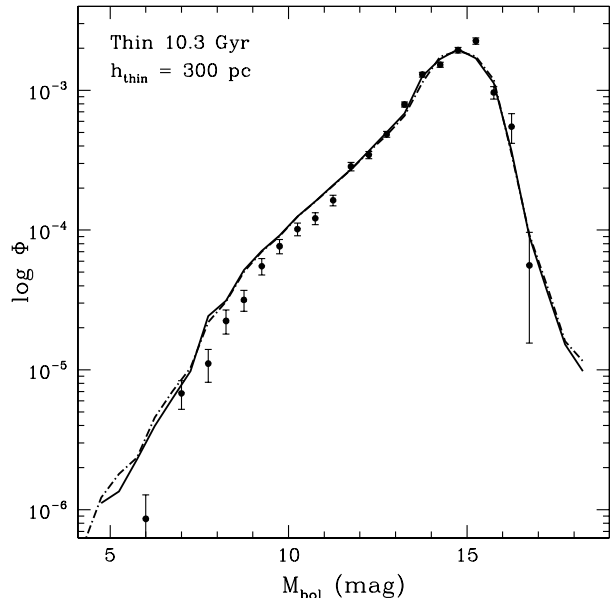


FIG. 3.— White dwarf luminosity function from the deep proper motion survey (points with error bars, Munn et al. 2017) assuming thin and thick disk scale heights of 300 and 900 pc, respectively. The solid and dot-dashed lines show the best-fitting model luminosity functions for a 100% thin disk population using the Kalirai et al. (2008) and Williams et al. (2009) initial-final mass relations, respectively.

tion from subdwarfs (at the low velocity end), they limit their disk sample to objects with $v_{\text{tan}} = 40-120 \text{ km s}^{-1}$. The 40 pc white dwarf sample contains 84 objects with $M_{\text{bol}} > 15$ mag, whereas the Munn et al. (2017) disk luminosity function has 311 objects in the same magnitude range. Hence, the latter survey significantly increases the number of stars beyond the turnover in the disk luminosity function, and it provides an excellent opportunity to disentangle the thin disk and thick disk luminosity functions.

Figure 3 presents the disk luminosity function from Munn et al. (2017) using the preferred disk model of Jurić et al. (2008) with thin and thick disk scale heights of 300 and 900 pc, respectively, and a thick to thin disk ratio of 12%. As in the analysis of the 40 pc luminosity function, we only use the stars with $M_{\text{bol}} > 11$ mag in our fits. Assuming a population of thin disk stars only, the best fit disk age is $10.3^{+0.3}_{-0.1}$ Gyr. The best-fitting disk model underpredicts the peak of the luminosity function, which is likely due to the missing contribution of thick disk stars in these fits. However, what is striking is that the models also overpredict the number of stars brighter than $M_{\text{bol}} = 11$ mag. The dashed-dotted line shows the same model luminosity function using the Williams et al. (2009, instead of Kalirai et al. 2008) initial-final mass relation. The difference between these two model luminosity functions is negligible. Hence, the choice of initial-final mass relation cannot explain the discrepancy between the observed and theoretical luminosity functions.

Harris et al. (2006) chose a disk scale height of 250 pc in their analysis, and they demonstrate (see their Figure 6) that changing the scale height from 200 to 350 pc has a significant impact on the shape of the luminosity function at the bright end. However, a constant scale height for

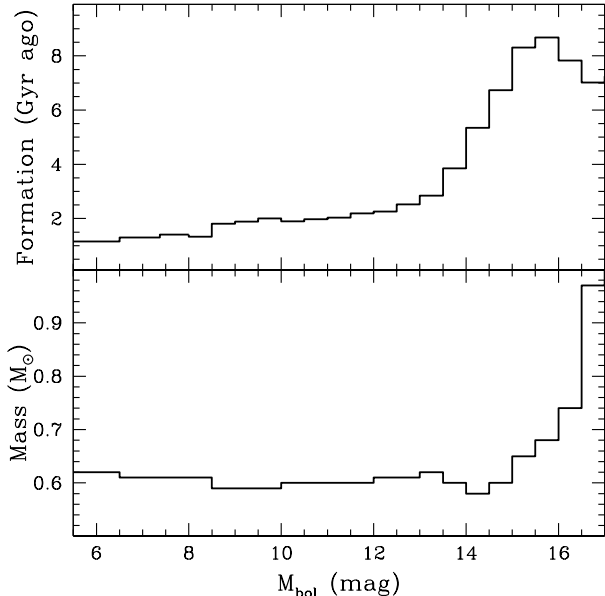


FIG. 4.— The median formation times for the progenitor stars and the median masses for the white dwarfs in each magnitude bin of the synthetic luminosity function for a 10.0 Gyr old thin disk population.

the entire disk is an over-simplification. In what follows, we develop a more realistic scaleheight correction for the disk luminosity function.

Bonatto et al. (2006) demonstrate that the scale height increases from 48 ± 3 pc for open clusters younger than 200 Myr to 150 ± 27 pc for clusters with ages up to 1 Gyr. Studying a larger sample of open clusters, Buckner & Froebrich (2014) and Joshi et al. (2016) show that this trend continues for older clusters; they find a scale height $h > 300$ pc for 2.5 Gyr and older clusters.

Bovy et al. (2012) use SEGUE G dwarfs to define mono-abundance populations, and fit each population as a single exponential disk. The scale height for these populations varies smoothly from around 200 pc for the most metal rich population to about 900 pc for the most metal poor population. They interpret the decreasing metallicity as an indication of increasing age, and their 900 pc limit is consistent with the thick disk scale height found by Jurić et al. (2008).

Figure 4 shows the median formation times of the progenitor main-sequence stars and median masses for the white dwarfs in each magnitude bin of a 10.0 Gyr old thin disk luminosity function. Based on our synthetic luminosity functions, the median formation times range from 1.2 Gyr at $M_{\text{bol}} = 6$ mag to 8.3 Gyr at $M_{\text{bol}} = 15.25$ mag. Thus, instead of a constant disk scale height, we let the scale height vary linearly between 200 pc for age = 1 Gyr to 900 pc for age = 10 Gyr.

Table 1 and Figure 5 compare the luminosity function with that age/scale-height relation applied to the median ages that we obtain. For comparison, we also overplot the preferred model from Munn et al. (2017, where $h_{\text{thin}} = 300$ pc), along with luminosity functions where the upper limit in scale height is 700 and 500 pc. The variable scale-height luminosity functions shown in Fig. 5 and Table 1 are consistent within the errors, but in

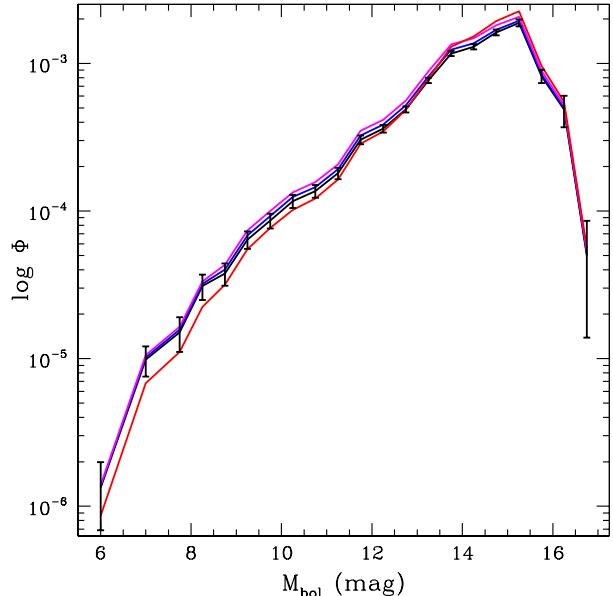


FIG. 5.— Luminosity functions using the Jurić et al. (2008) disk model (red), and models with scale heights that vary linearly with age from 200 pc at 1 Gyr to 500 (magenta), 700 (blue), and 900 pc (black) at 10 Gyr.

the $M_{\text{bol}} < 11$ mag range they have a significantly larger space density than the luminosity function assuming a constant thin disk scale height of 300 pc. Hence, the discrepancy between the observed and model luminosity functions in Figure 3 is likely due to our previous assumption of a constant scale height for the disk.

4.2. Thin Disk and Thick Disk Ages

Following the discussion from Section 3.2, the expected white dwarf number density is $\rho_{\text{thick}}/\rho_{\text{thin}} = 21.7\%$ for a kinematically unbiased population. Munn et al. (2017) correct the disk luminosity function for missing objects with $V_{\text{tan}} < 40$ or > 120 km s $^{-1}$ using the modified maximum survey volume of Lam et al. (2015) as the density estimator. However, they treat the disk objects as a single population, and sum the thin and thick disk profiles of Jurić et al. (2008) as a single disk density profile and use the Fuchs et al. (2009) results to model the kinematics of the disk. Hence, they correct for the overall number of disk objects in their survey, but these corrections do not include the change in the relative numbers of thin and thick disk objects due to the $V_{\text{tan}} = 40\text{-}120$ km s $^{-1}$ cut.

The median Galactic latitude of the fields observed by Munn et al. (2017) is $|b| = 50^\circ$, with the range $34^\circ\text{-}63^\circ$ containing 68% of the observed fields. Based on the Besançon Galaxy model for $|b| = 50^\circ$, we expect 59.1% and 33.7% of thin disk and thick disk stars to be lost due to the 40-120 km s $^{-1}$ tangential velocity cut. Hence, the expected ratio of thick versus thin disk white dwarfs in the deep proper motion survey disk luminosity function is 35.2%. Using the $|b| = 34^\circ\text{-}63^\circ$ range, the expected ratio is between 32.2 and 41.6%, with an additional 3-4% uncertainty due to the density uncertainty estimates from Jurić et al. (2008).

Figure 6 shows the white dwarf luminosity function

TABLE 1
 WHITE DWARF LUMINOSITY FUNCTIONS USING DIFFERENT SCALE HEIGHTS

M_{bol} (mag)	$\Phi_{200-900}$ ($\text{pc}^{-3} M_{\text{bol}}^{-1}$)	$\Phi_{200-700}$ ($\text{pc}^{-3} M_{\text{bol}}^{-1}$)	$\Phi_{200-500}$ ($\text{pc}^{-3} M_{\text{bol}}^{-1}$)	$\Phi_{\text{Munn et al. (2017)}}$ ($\text{pc}^{-3} M_{\text{bol}}^{-1}$)
6.00	$1.337\text{e-}06 \pm 6.487\text{e-}07$	$1.366\text{e-}06 \pm 6.628\text{e-}07$	$1.396\text{e-}06 \pm 6.775\text{e-}07$	$8.196\text{e-}07 \pm 3.945\text{e-}07$
7.00	$9.838\text{e-}06 \pm 2.284\text{e-}06$	$1.018\text{e-}05 \pm 2.364\text{e-}06$	$1.054\text{e-}05 \pm 2.450\text{e-}06$	$6.888\text{e-}06 \pm 1.536\text{e-}06$
7.75	$1.509\text{e-}05 \pm 3.998\text{e-}06$	$1.573\text{e-}05 \pm 4.169\text{e-}06$	$1.644\text{e-}05 \pm 4.358\text{e-}06$	$1.219\text{e-}05 \pm 3.006\text{e-}06$
8.25	$3.104\text{e-}05 \pm 6.105\text{e-}06$	$3.212\text{e-}05 \pm 6.319\text{e-}06$	$3.330\text{e-}05 \pm 6.551\text{e-}06$	$2.236\text{e-}05 \pm 4.313\text{e-}06$
8.75	$3.768\text{e-}05 \pm 6.498\text{e-}06$	$4.020\text{e-}05 \pm 6.932\text{e-}06$	$4.328\text{e-}05 \pm 7.464\text{e-}06$	$3.656\text{e-}05 \pm 5.699\text{e-}06$
9.25	$6.406\text{e-}05 \pm 8.585\text{e-}06$	$6.845\text{e-}05 \pm 9.174\text{e-}06$	$7.394\text{e-}05 \pm 9.910\text{e-}06$	$5.464\text{e-}05 \pm 7.222\text{e-}06$
9.75	$8.614\text{e-}05 \pm 9.988\text{e-}06$	$9.231\text{e-}05 \pm 1.070\text{e-}05$	$1.002\text{e-}04 \pm 1.162\text{e-}05$	$8.218\text{e-}05 \pm 9.003\text{e-}06$
10.25	$1.167\text{e-}04 \pm 1.208\text{e-}05$	$1.243\text{e-}04 \pm 1.287\text{e-}05$	$1.338\text{e-}04 \pm 1.385\text{e-}05$	$1.097\text{e-}04 \pm 1.071\text{e-}05$
10.75	$1.363\text{e-}04 \pm 1.336\text{e-}05$	$1.452\text{e-}04 \pm 1.424\text{e-}05$	$1.567\text{e-}04 \pm 1.536\text{e-}05$	$1.237\text{e-}04 \pm 1.183\text{e-}05$
11.25	$1.802\text{e-}04 \pm 1.580\text{e-}05$	$1.919\text{e-}04 \pm 1.682\text{e-}05$	$2.069\text{e-}04 \pm 1.813\text{e-}05$	$1.680\text{e-}04 \pm 1.431\text{e-}05$
11.75	$3.042\text{e-}04 \pm 2.082\text{e-}05$	$3.241\text{e-}04 \pm 2.219\text{e-}05$	$3.504\text{e-}04 \pm 2.400\text{e-}05$	$2.972\text{e-}04 \pm 1.964\text{e-}05$
12.25	$3.615\text{e-}04 \pm 2.123\text{e-}05$	$3.842\text{e-}04 \pm 2.256\text{e-}05$	$4.144\text{e-}04 \pm 2.434\text{e-}05$	$3.556\text{e-}04 \pm 2.029\text{e-}05$
12.75	$4.882\text{e-}04 \pm 2.352\text{e-}05$	$5.192\text{e-}04 \pm 2.501\text{e-}05$	$5.614\text{e-}04 \pm 2.704\text{e-}05$	$5.044\text{e-}04 \pm 2.353\text{e-}05$
13.25	$7.675\text{e-}04 \pm 3.213\text{e-}05$	$8.154\text{e-}04 \pm 3.413\text{e-}05$	$8.817\text{e-}04 \pm 3.691\text{e-}05$	$8.164\text{e-}04 \pm 3.334\text{e-}05$
13.75	$1.166\text{e-}03 \pm 4.525\text{e-}05$	$1.237\text{e-}03 \pm 4.801\text{e-}05$	$1.345\text{e-}03 \pm 5.220\text{e-}05$	$1.345\text{e-}03 \pm 5.072\text{e-}05$
14.25	$1.296\text{e-}03 \pm 5.325\text{e-}05$	$1.367\text{e-}03 \pm 5.612\text{e-}05$	$1.482\text{e-}03 \pm 6.086\text{e-}05$	$1.565\text{e-}03 \pm 6.320\text{e-}05$
14.75	$1.620\text{e-}03 \pm 7.352\text{e-}05$	$1.691\text{e-}03 \pm 7.674\text{e-}05$	$1.815\text{e-}03 \pm 8.232\text{e-}05$	$1.961\text{e-}03 \pm 8.793\text{e-}05$
15.25	$1.881\text{e-}03 \pm 9.947\text{e-}05$	$1.947\text{e-}03 \pm 1.030\text{e-}04$	$2.066\text{e-}03 \pm 1.093\text{e-}04$	$2.292\text{e-}03 \pm 1.197\text{e-}04$
15.75	$8.211\text{e-}04 \pm 8.394\text{e-}05$	$8.453\text{e-}04 \pm 8.641\text{e-}05$	$8.888\text{e-}04 \pm 9.087\text{e-}05$	$9.945\text{e-}04 \pm 9.927\text{e-}05$
16.25	$4.860\text{e-}04 \pm 1.171\text{e-}04$	$4.981\text{e-}04 \pm 1.199\text{e-}04$	$5.194\text{e-}04 \pm 1.247\text{e-}04$	$5.568\text{e-}04 \pm 1.315\text{e-}04$
16.75	$4.990\text{e-}05 \pm 3.602\text{e-}05$	$5.124\text{e-}05 \pm 3.698\text{e-}05$	$5.353\text{e-}05 \pm 3.863\text{e-}05$	$5.591\text{e-}05 \pm 4.034\text{e-}05$

from the deep proper motion survey using a variable disk scale height of 200-900 pc. The top panel shows our fits assuming a population of thin disk stars only, which leads to an age estimate of 9.9 Gyr. Interestingly, the observed and best-fitting model luminosities agree within 2.3σ in the $M_{\text{bol}} = 7-13$ mag range. Accounting for a disk scale height that increases with age yields luminosity functions consistent with a constant star formation rate in the past ~ 2.5 Gyr.

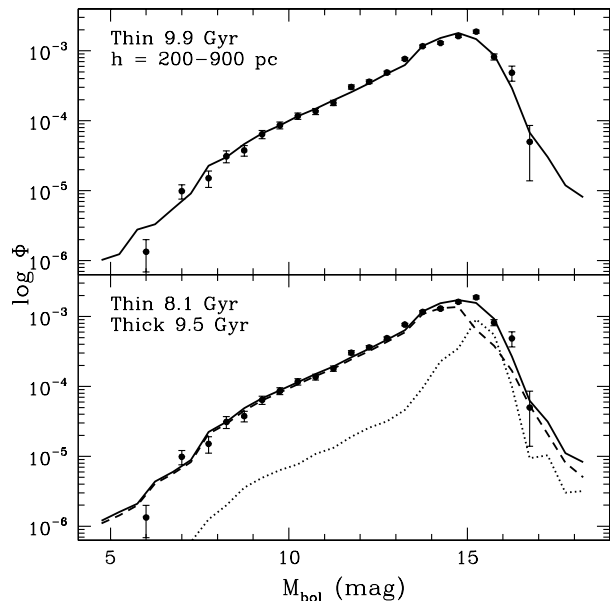


FIG. 6.— The white dwarf luminosity function from the deep proper motion survey (points with error bars, Munn et al. 2017) using a disk scale height range of 200-900 pc. The top panel shows the model fits assuming a population of 100% thin disk stars, whereas the bottom panel shows the fits using a composite population where the ratio of thick disk to thin disk white dwarfs is 35%. Dashed and dotted lines show the contribution from the thin disk and thick disk white dwarfs, respectively.

The bottom panel in Figure 6 shows the best-fitting thin disk + thick disk composite luminosity function for $\rho_{\text{thick,WD}}/\rho_{\text{thin,WD}} = 35\%$. The best-fitting model has ages of $8.1^{+0.2}_{-0.1}$ Gyr and 9.5 ± 0.2 Gyr for the thin disk and thick disk, respectively. The composite thin+thick disk model matches the peak of the luminosity function relatively well.

Figure 7 shows age constraints on the thin and thick disk as a function of the number density of thick versus thin disk white dwarfs. We use the same color-scheme as in Figure 5 to indicate the models with different scale heights. This figure demonstrates that the thick disk age is constrained relatively well to 9.5 ± 0.2 Gyr, even in the luminosity function that uses a constant disk scale height

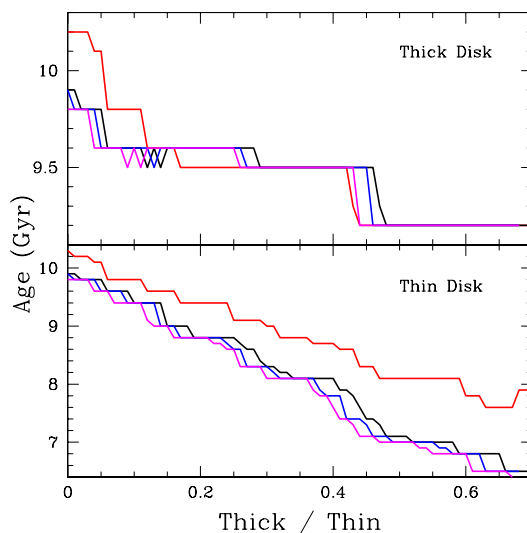


FIG. 7.— Thin disk and thick disk age constraints as a function of the ratio of thick disk to thin disk white dwarfs. The black, blue, magenta, and red lines show the constraints from luminosity functions using the scale heights of 200-900 pc (Bovy et al. 2012), 200-700 pc, 200-500 pc, and 300 pc (Jurić et al. 2008), respectively.

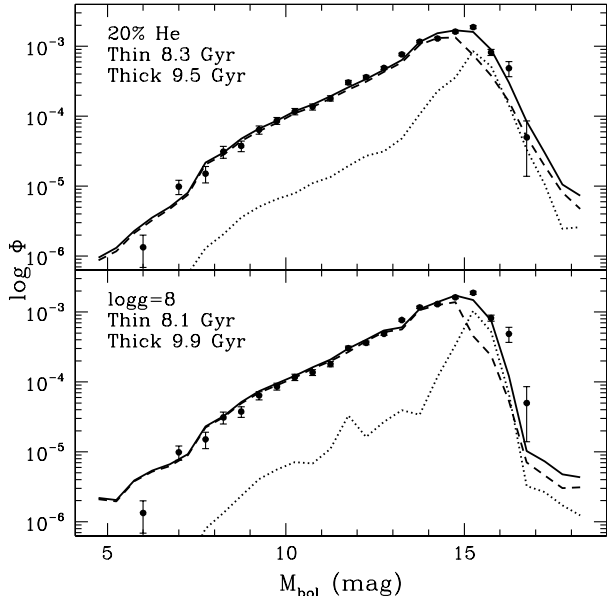


FIG. 8.— Fits to the disk luminosity function assuming that 20% of the white dwarfs have pure Helium atmospheres (top panel), or 100% of them have $\log g = 8$ (bottom panel). Dashed and dotted lines show the contribution from the thin disk and thick disk white dwarfs, assuming a 35% thick/thin ratio, respectively.

of 300 pc. This is because the thick disk is an old population, and most of the age sensitivity comes from the observed cut-off in the luminosity function, which does not vary considerably between the different luminosity functions presented in Figure 5. On the other hand, the thin disk age measurement heavily depends on the shape of the broad peak observed above $M_{\text{bol}} = 13$ mag and it is sensitive to the assumed thick/thin disk population fraction. For a thick/thin ratio of 35%, the age of the thin disk is 8.1 Gyr for models that use a variable scale height. However, the thin disk age varies from 7.4 to 8.2 Gyr for a thick/thin ratio in the range 32%–42%. Hence, based on the Munn et al. (2017) disk luminosity function, we adopt an age of 7.4–8.2 Gyr for the thin disk.

4.3. Thin Disk and Thick Disk Ages: Caveats

There are two caveats in our analysis of the disk ages. The first one is the assumed fractions of hydrogen versus helium atmosphere white dwarfs in our synthetic luminosity functions. Based on the analysis of Kowalski & Saumon (2006), we assumed a 100% fraction of H atmosphere white dwarfs in our analysis. Torres & García-Berro (2016) use fractions of 80% DA and 20% DB in their analysis of the 40 pc sample. To explore the effects of DB white dwarfs on our age measurements, we repeat our analysis of the disk luminosity function assuming a DB white dwarf fraction of 20%.

Figure 8 shows these fits using a 20% pure He atmosphere fraction for both the thin disk and thick disk populations (top panel). For a ratio of $\rho_{\text{thick}}/\rho_{\text{thin}} = 35\%$, the best-fitting model has ages of $8.3^{+0.3}_{-0.2}$ Gyr and $9.5^{+0.1}_{-0.3}$ Gyr for the thin disk and thick disk, respectively. These are consistent with our previous disk age estimates within 1σ . Hence, the choice of DA versus DB atmospheres has a negligible effect on our age measurements for a DB white dwarf fraction of $\sim 20\%$.

Due to the lack of parallax measurements, Munn et al. (2017) had to assume $\log g = 8$ for all stars in their sample. This is the second caveat in our analysis as our synthetic luminosity functions draw stars with random initial masses from a Salpeter mass function and use the initial-final mass relation to estimate the white dwarf masses. The bottom panel in Figure 4 shows the median masses for the white dwarfs in each magnitude bin of the synthetic luminosity function for a 10 Gyr old thin disk population. The median mass ranges between 0.58 and $0.62 M_{\odot}$ for $M_{\text{bol}} < 15$ mag. Hence, the assumption of $\log g = 8$ is appropriate for getting the overall shape of the luminosity function right. However, the median mass increases to $\approx 0.7 M_{\odot}$ at $M_{\text{bol}} = 16$ mag, which has implications for the age measurements from the faint end of the luminosity function.

Munn et al. (2017) fit the SDSS photometry of each target with the $\log g = 8$ white dwarf models to derive its T_{eff} and bolometric magnitude. To explore the effects of the $\log g = 8$ assumption on our age estimates, we create synthetic luminosity functions where we use the cooling age of each white dwarf to estimate its T_{eff} , and calculate its bolometric luminosity at that temperature assuming $\log g = 8$. The bottom panel in Figure 8 shows these fits for $\log g = 8$ white dwarfs. The best-fitting model has ages of $8.1^{+0.2}_{-0.1}$ Gyr and 9.9 ± 0.1 Gyr for the thin disk and thick disk, respectively.

The thin disk age is essentially unchanged from our previous estimates, as the peak of the thin disk luminosity function is below $M_{\text{bol}} = 15$ mag, where the median mass in our synthetic luminosity functions is around $0.6 M_{\odot}$. However, the thick disk age is sensitive to the magnitude bins where the median mass is $\approx 0.7 M_{\odot}$. Based on the Fontaine et al. (2001) cooling models, a $4,000$ K, $0.7 M_{\odot}$ white dwarf has a bolometric magnitude of 16.1, whereas a $0.6 M_{\odot}$ white dwarf at the same temperature has $M_{\text{bol}} = 15.9$ mag. Hence, the assumption of $\log g = 8$ underestimates the bolometric magnitudes of the white dwarfs at the faint end of the luminosity function. This requires a larger age for our targets to reach the observed cut-off in magnitude. Given this systematic uncertainty in age, we adopt a best-fit age of 9.5–9.9 Gyr for the thick disk.

4.4. The Halo Luminosity Function

Previous efforts to create halo white dwarf luminosity functions using field stars have suffered from small number statistics. For example, Harris et al. (2006) identify 18 stars with $v_{\text{tan}} > 200$ km s $^{-1}$ as halo white dwarf candidates, including two stars with $M_{\text{bol}} > 14$ mag. Rowell & Hambly (2011) find 93 stars with $v_{\text{tan}} > 200$ km s $^{-1}$ and UVW space velocities that are consistent with a non-rotating population (the spheroid). Their luminosity function includes objects as faint as $M_{\text{bol}} = 15$ mag, though the faint end of their luminosity function has relatively large error bars due to small numbers of stars in those magnitude bins.

Munn et al. (2017) use 135 stars with $M_{\text{bol}} = 5.5 - 17$ mag to create a halo white dwarf luminosity function. To minimize the contamination from the large number of disk objects, they limit their halo sample to objects with $v_{\text{tan}} = 200\text{--}500$ km s $^{-1}$. Figure 9 shows this luminosity function, which contains 21 stars with $M_{\text{bol}} = 14\text{--}16$ mag.

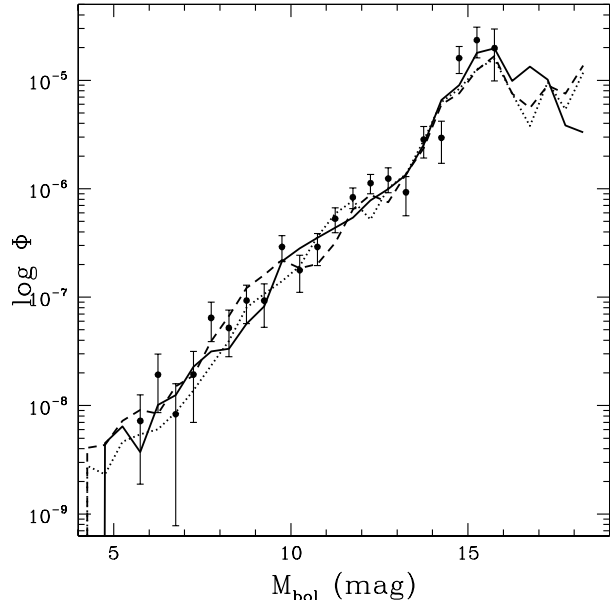


FIG. 9.— Munn et al. (2017) luminosity function for $v_{\text{tan}} = 200$ –500 km s^{-1} halo white dwarf sample. Solid, dashed, and dotted lines show model luminosity functions for 12.5, 13.9, and 15.0 Gyr old halo samples, respectively. This luminosity function implies a halo age of $12.5^{+1.4}_{-3.4}$ Gyr.

The halo white dwarf luminosity function rises nearly monotonically to $M_{\text{bol}} = 16$ mag, though the turnover at the faint end remains undetected. Fitting this luminosity function with our models based on a Salpeter initial mass function, star formation in the first Gyr after its formation, Hurley et al. (2000) main-sequence lifetimes for metal-poor stars, Kalirai et al. (2008) initial-final mass relation, Fontaine et al. (2001) evolutionary models, and based on 10,000 Monte-Carlo simulations, we find that the halo age is constrained to ≥ 8.1 Gyr at the 99.7% confidence level (3σ). The best-fit halo age is $12.5^{+1.4}_{-3.4}$ Gyr, and the 1σ upper limit of 13.9 Gyr is consistent with the latest constraints on the age of the Universe (Planck Collaboration et al. 2016). However, this luminosity function is not deep enough to show a cutoff at the faint end, and is consistent with an arbitrarily large halo age of 15.0 Gyr (the upper age limit of our model luminosity functions) within 2σ .

Figure 9 shows the best-fitting model (12.5 Gyr, solid line) luminosity function, as well as the models for 13.9 Gyr (dashed) and 15.0 Gyr (dotted line) old halo. Our halo age estimate is consistent with the age measurements for the inner halo from the field halo white dwarfs of Kalirai (2012, 11.4 ± 0.7 Gyr), Kilic et al. (2012, 11–11.5 Gyr), and Si et al. (2017, $11.67^{+1.02}_{-0.96}$ Gyr), as well as the ages of the globular cluster white dwarf sequences of M4, NGC 6397, and 47 Tuc, which span a range of 9.9 to 11.5 Gyr. However, better age constraints for the inner halo would require a luminosity function that goes at least a magnitude deeper than the current surveys.

5. CONCLUSIONS

We present an analysis of the white dwarf luminosity functions from the local 40 pc sample and the deep proper motion survey of Munn et al. (2017). We demon-

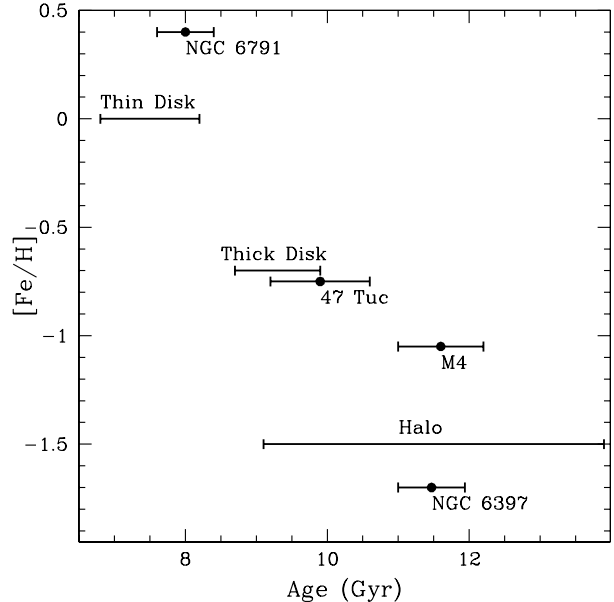


FIG. 10.— Age-Metallicity relation based on the white dwarf luminosity functions for the open cluster NGC 6791, globular clusters 47 Tuc, M4, and NGC 6397 (Hansen et al. 2013, and references therein), and field thin disk, thick disk, and halo stars from this study. The error bars cover the age ranges estimated from both the 40 pc local sample and the Munn et al. (2017) deep proper motion survey sample.

strate that both samples have significant numbers of thick disk stars that define the faint end of their luminosity functions. Simultaneously fitting for both disk components, we constrain the ages of the thin disk and thick disk to be 6.8–7.0 Gyr and 8.7 ± 0.1 Gyr from the local sample, and 7.4–8.2 Gyr and 9.5–9.9 Gyr from the Munn et al. (2017) sample of white dwarfs, respectively.

Figure 10 presents the age-metallicity relation based on the white dwarf luminosity functions for four clusters studied with the *Hubble Space Telescope* (Hansen et al. 2013). This figure also includes our results from field white dwarfs. Our thin disk age estimate of 6.8–8.2 Gyr is larger than the ages of the oldest, solar-metallicity open clusters observed, e.g. M67 (4 Gyr, Sandquist 2004; von Hippel 2005) and NGC 188 (6.2 Gyr, Meibom et al. 2009). However, this is not surprising, since older clusters are tidally disrupted over the lifetime of the disk (Soderblom 2010). In addition, this age is in excellent agreement with the 7.3 ± 1.5 Gyr age estimate from the Liebert et al. (1988) white dwarf luminosity function by Hansen et al. (2002), as well as the ages of 8.0 ± 0.4 Gyr for the metal-rich cluster NGC 6791 (García-Berro et al. 2010) and 7.5 – 7.9 ± 0.7 Gyr for the turn-off field stars and subgiants with parallax measurements (Liu & Chaboyer 2000; Sandage et al. 2003). Our thick disk age measurements from the 40 pc and the Munn et al. (2017) sample differ significantly, but the latter survey includes white dwarfs with estimated distances of up to ~ 1 kpc. There is a well established trend between the age of a population and its disk scale height (e.g., Bovy et al. 2012), hence the relatively younger ages estimated from the local 40 pc sample are not surprising. The observed age range of 8.7–9.9 Gyr for thick disk white dwarfs is in excellent agreement with the relatively metal-rich globular

cluster 47 Tuc (Hansen et al. 2013).

Perhaps the most important result of this analysis is not the absolute age measurements, but instead the demonstration of age differences between the different kinematic populations of white dwarfs. For the 40 pc local sample, we measure relative age differences of 1.9 ± 0.2 Gyr and $1.6_{-0.1}^{+0.2}$ Gyr between the thin disk and thick disk populations based on the original luminosity function presented by Limoges et al. (2015) and the same luminosity function with the shifted bin centers (see §3.3). Similarly, our analysis of the disk luminosity function from the deep proper motion survey implies a relative age difference of $1.4_{-0.3}^{+0.1}$ Gyr. Combining the results for the local 40 pc sample and the Munn et al. (2017) proper motion sample, we constrain the time between the onset of star formation in the thick disk and thin disk to be $1.6_{-0.4}^{+0.3}$ Gyr. This is similar to, though twice as precise as, the relative age difference of 1.9 ± 0.8 Gyr between 47 Tuc and NGC 6791.

Accurate parallaxes from the Gaia mission will help in constraining the faint end of the disk luminosity function. In addition, where radial velocity measurements are also available, Gaia data will help separate thin and thick disk objects based on their 3D space velocities. However, the peak of the thick disk luminosity function is beyond $M_{\text{bol}} = 15$ mag and $T_{\text{eff}} = 5000$ K, below which H α disappears. Hence, it is likely that future studies of the Gaia disk luminosity function will have to rely on a method similar to ours (or to Rowell & Hambly 2011; Lam 2017) in disentangling the thin disk and thick disk luminosity functions.

Both Limoges et al. (2015) and Torres & García-Berro

(2016) find evidence of an enhanced star formation rate in the past 300-600 Myr in the local 40 pc white dwarf sample. On the other hand, we do not find any evidence of a deviation from a constant star formation rate in the past 2.5 Gyr in the Munn et al. (2017) disk luminosity function, which samples a more distant population of white dwarfs. Most molecular clouds and star formation are constrained close to the Galactic plane. The scale height for open clusters younger than 200 Myr is only 48 pc (Bonatto et al. 2006). Hence, we conclude that the enhanced star formation rate observed in the 40 pc local sample is only relevant for the immediate Solar neighborhood. Gaia parallaxes will enable us to create disk luminosity functions as a function of distance and study their star formation histories.

The faint end of the luminosity function for nearby halo white dwarfs is not constrained reliably, leading to an age estimate of $12.5_{-3.4}^{+1.4}$ Gyr. Large scale surveys that reach at least 1 mag deeper than the Munn et al. (2014) proper motion survey will be useful for better constraining the halo luminosity function. The Large Synoptic Survey Telescope (LSST) will image 13 million white dwarfs down to $r = 24.5$ mag. Munn et al. (2017) measure a space density of 1/157 for halo/disk white dwarfs. Even with such a small density, the LSST will identify $\sim 10^5$ halo white dwarfs, which will enable precise age estimates for the inner halo.

We gratefully acknowledge the support of the NSF and NASA under grants AST-0607480, AST-0602288, AST-1312678, and NNX14AF65G.

REFERENCES

- Althaus, L. G., García-Berro, E., Isern, J., Córscico, A. H., & Rohrmann, R. D. 2007, *A&A*, 465, 249
- Angus, R., Aigrain, S., Foreman-Mackey, D., & McQuillan, A. 2015, *MNRAS*, 450, 1787
- Barnes, S. A., Weingrill, J., Fritzewski, D., Strassmeier, K. G., & Platais, I. 2016, *ApJ*, 823, 16
- Bergeron, P., Leggett, S. K., & Ruiz, M. T. 2001, *ApJS*, 133, 413
- Bonatto, C., Kerber, L. O., Bica, E., & Santiago, B. X. 2006, *A&A*, 446, 121
- Bovy, J., Rix, H.-W., & Hogg, D. W. 2012, *ApJ*, 751, 131
- Buckner, A. S. M., & Froebrich, D. 2014, *MNRAS*, 444, 290
- Catalán, S., Isern, J., García-Berro, E., et al. 2008, *A&A*, 477, 213
- Cignoni, M., Degl'Innocenti, S., Prada Moroni, P. G., & Shore, S. N. 2006, *A&A*, 459, 783
- de Jong, J. T. A., Yanny, B., Rix, H.-W., et al. 2010, *ApJ*, 714, 663
- Fontaine, G., Brassard, P., & Bergeron, P. 2001, *PASP*, 113, 409
- Frebel, A., Christlieb, N., Norris, J. E., et al. 2007, *ApJ*, 660, L117
- Fuchs, B., Dettbarn, C., Rix, H.-W., et al. 2009, *AJ*, 137, 4149
- García-Berro, E., Torres, S., Althaus, L. G., et al. 2010, *Nature*, 465, 194
- Hansen, B. M. S., Brewer, J., Fahlman, G. G., et al. 2002, *ApJ*, 574, L155
- Hansen, B. M. S., Richer, H. B., Fahlman, G. G., et al. 2004, *ApJS*, 155, 551
- Hansen, B. M. S., Anderson, J., Brewer, J., et al. 2007, *ApJ*, 671, 380
- Hansen, B. M. S., Kalirai, J. S., Anderson, J., et al. 2013, *Nature*, 500, 51
- Harris, H. C., Munn, J. A., Kilic, M., et al. 2006, *AJ*, 131, 571
- Hurley, J. R., Pols, O. R., & Tout, C. A. 2000, *MNRAS*, 315, 543
- Ivezić, Ž., Sesar, B., Jurić, M., et al. 2008, *ApJ*, 684, 287-325
- Joshi, Y. C., Dambis, A. K., Pandey, A. K., & Joshi, S. 2016, *A&A*, 593, A116
- Jurić, M., Ivezić, Ž., Brooks, A., et al. 2008, *ApJ*, 673, 864
- Kalirai, J. S., Hansen, B. M. S., Kelson, D. D., et al. 2008, *ApJ*, 676, 594
- Kalirai, J. S. 2012, *Nature*, 486, 90
- Kilic, M., Thorstensen, J. R., Kowalski, P. M., & Andrews, J. 2012, *MNRAS*, 423, L132
- Kowalski, P. M., & Saumon, D. 2006, *ApJ*, 651, L137
- Lam, M. C., Rowell, N., & Hambly, N. C. 2015, *MNRAS*, 450, 4098
- Lam, M. C. 2017, PhD Thesis, The University of Edinburgh
- Leggett, S. K., Ruiz, M. T., & Bergeron, P. 1998, *ApJ*, 497, 294
- Liebert, J., Dahn, C. C., & Monet, D. G. 1988, *ApJ*, 332, 891
- Limoges, M.-M., Bergeron, P., & Lépine, S. 2015, *ApJS*, 219, 19
- Liu, W. M., & Chaboyer, B. 2000, *ApJ*, 544, 818
- Meibom, S., Grundahl, F., Clausen, J. V., et al. 2009, *AJ*, 137, 5086
- Munn, J. A., Monet, D. G., Levine, S. E., et al. 2004, *AJ*, 127, 3034
- Munn, J. A., Harris, H. C., von Hippel, T., et al. 2014, *AJ*, 148, 132
- Munn, J. A., Harris, H. C., von Hippel, T., et al. 2017, *AJ*, 153, 10
- Pauli, E.-M., Napiwotzki, R., Heber, U., Altmann, M., & Odenkirchen, M. 2006, *A&A*, 447, 173
- Planck Collaboration, Ade, P. A. R., Aghanim, N., et al. 2016, *A&A*, 594, A13
- Reid, I. N. 2005, *ARA&A*, 43, 247
- Renedo, I., Althaus, L. G., Miller Bertolami, M. M., et al. 2010, *ApJ*, 717, 183
- Robin, A. C., Reylé, C., Marshall, D. J., & Schultheis, M. 2012, *Astrophysics and Space Science Proceedings*, 26, 171
- Rowell, N., & Hambly, N. C. 2011, *MNRAS*, 417, 93
- Salpeter, E. E. 1955, *ApJ*, 121, 161
- Sandage, A., Lubin, L. M., & Vandenberg, D. A. 2003, *PASP*, 115, 1187
- Sandquist, E. L. 2004, *MNRAS*, 347, 101
- Schwarzschild, M. 1958, Princeton, Princeton University Press, 1958
- Si, S., van Dyk D. A., von Hippel, T., Robinson, E., Webster, A., & Stenning, D. 2017, *MNRAS*, submitted
- Snedden, C., Cowan, J. J., Lawler, J. E., et al. 2003, *ApJ*, 591, 936
- Soderblom, D. R. 2010, *ARA&A*, 48, 581
- Torres, S., & García-Berro, E. 2016, *A&A*, 588, A35
- Tremblay, P.-E., Kalirai, J. S., Soderblom, D. R., Cignoni, M., & Cummings, J. 2014, *ApJ*, 791, 92

von Hippel, T. 2005, ApJ, 622, 565
Williams, K. A., Bolte, M., & Koester, D. 2009, ApJ, 693, 355

Winget, D. E., Hansen, C. J., Liebert, J., et al. 1987, ApJ, 315,
L77